Acta Biomaterialia 121 (2021) 303–315

Contents lists available at ScienceDirect

Acta Biomaterialia

journal homepage: www.elsevier.com/locate/actbio

Development and characterisation of cytocompatible polyester substrates with tunable mechanical properties and degradation rate

Sofia Ribeiro[a,b,c], Ana M. Carvalho[d,e], Emanuel M. Fernandes[d,e], Manuela E. Gomes[d,e,f], Rui L. Reis[d,e,f], Yves Bayon[a], Dimitrios I. Zeugolis[b,c,g,*]

[a] Sofradim Production, Medtronic, Trevoux, France
[b] Regenerative, Modular & Developmental Engineering Laboratory (REMODEL), National University of Ireland Galway (NUI Galway), Galway, Ireland
[c] Science Foundation Ireland (SFI) Centre for Research in Medical Devices (CÚRAM) National University of Ireland Galway (NUI Galway), Galway, Ireland
[d] 3B's Research Group, I3Bs – Research Institute on Biomaterials, Biodegradables and Biomimetics, University of Minho, Headquarters of the European Institute of Excellence on Tissue Engineering and Regenerative Medicine, AvePark, Parque de Ciência e Tecnologia, Zona Industrial da Gandra, 4805-017 Barco, Guimarães, Portugal
[e] ICVS/3B's – PT Government Associate Laboratory, Braga / Guimarães, Portugal
[f] The Discoveries Centre for Regenerative and Precision Medicine, Headquarters at University of Minho, Avepark, 4805-017 Barco, Guimarães, Portugal
[g] Regenerative, Modular & Developmental Engineering Laboratory (REMODEL), Faculty of Biomedical Sciences, Università della Svizzera Italiana (USI), Lugano, Switzerland

ARTICLE INFO

Article history:
Received 8 August 2020
Revised 12 November 2020
Accepted 17 November 2020
Available online 20 November 2020

Keywords:
Biodegradable polyesters
Substrate stiffness
Physicochemical properties
Dermal fibroblast response
In vitro immune response

ABSTRACT

Although it has been repeatedly indicated the importance to develop implantable devices and cell culture substrates with tissue-specific rigidity, current commercially available products, in particular cell culture substrates, have rigidity values well above most tissues in the body. Herein, six resorbable polyester films were fabricated using compression moulding with a thermal presser into films with tailored stiffness by appropriately selecting the ratio of their building up monomers (e.g. lactide, glycolide, trimethylene carbonate, dioxanone, ε-caprolactone). Typical NMR and FTIR spectra were obtained, suggesting that the fabrication process did not have a negative effect on the conformation of the polymers. Surface roughness analysis revealed no apparent differences between the films as a function of polymer composition. Subject to polymer composition, polymeric films were obtained with glass transition temperatures from -52 °C to 61 °C; contact angles in water from 81 ° to 94 °; storage modulus from 108 MPa to 2,756 MPa and loss modulus from 8 MPa to 507 MPa (both in wet state, at 1 Hz frequency and at 37 °C); ultimate tensile strength from 8 MPa to 62 MPa, toughness from 23 MJ/m^3 to 287 MJ/m^3, strain at break from 3 % to 278 %, macro-scale Young's modulus from 110 MPa to 2,184 MPa (all in wet state); and nano-scale Young's modulus from 6 kPa to 15,019 kPa (in wet state). With respect to *in vitro* degradation in phosphate buffered saline at 37 °C, some polymeric films [e.g. poly(glycolide-lactide) 30 / 70] started degrading from day 7 (shortest timepoint assessed), whilst others [e.g. poly(glycolide-co-ε-caprolactone) 10 / 90] were more resilient to degradation up to day 21 (longest timepoint assessed). *In vitro* biological analysis using human dermal fibroblasts and a human monocyte cell line (THP-1) showed the potential of the polymeric films to support cell growth and controlled immune response. Evidently, the selected polymers exhibited properties suitable for a range of clinical indications.

Statement of significance

The submitted manuscript describes the development and structural, physicochemical and biological characterisation of six resorbable polyester films, produced using compression moulding with a thermal presser. Data obtained demonstrate that by appropriately selecting the ratio of the polymeric materials' building blocks (i.e. lactic acid, glycolic acid, trimethylene carbonate, dioxanone, ε-caprolactone monomers), substrates with tunable biochemical, biophysical and biological properties can be fabricated to match the properties of a wide range of tissues and cells thereof.

https://doi.org/10.1016/j.actbio.2020.11.026

1. Introduction

The use of synthetic biodegradable polymers [e.g. poly(ε-caprolactone) [1], poly(glycolide) [2], poly(lactide) [3], poly(dioxanone) [4], poly(trimethylene carbonate) [5]] and copolymers thereof [e.g. poly(glycolide-co-ε-caprolactone), poly(glycolide-co-dioxanone-co-trimethylene carbonate), poly(lactide-co-trimethylene carbonate), poly(lactide-co-glycolide)] has been advocated for tissue engineering and drug delivery purposes for their acceptable cytocompatibility, batch-to-batch reproducibility, controllable biodegradability, tailored mechanical properties and relatively easy processability to tissue-mimetic three-dimensional conformations in a cost effective manner [6,7]. Indeed, aliphatic polyesters and their copolymers constitute the building blocks of a large number of medical devices (e.g. sutures, absorbable orthopaedic implants, wound healing devices) approved by FDA and EMA, with diverse range of degradation and mechanical properties, fulfilling that way drug delivery and remodelling needs for most, if not all, biomedical applications [8–12].

Tissue or cell / biomaterial mechanical properties mismatch is still a major issue in biomedical engineering. Indeed, tissue/device mechanical properties mismatch [13–16] is often associated with implant failure. In cell therapies, although the importance of substrate elasticity on cell adhesion, morphology, proliferation, migration, gene expression, protein synthesis and lineage commitment has been well documented [17,18], traditional cell cultures are conducted on polystyrene tissue culture plastic (TCP) that fails to mimic most tissues elastic modulus (e.g. 3.5-25.9 kPa pituitary gland [19], 0.01 MPa buttock-thigh tissue [20], 0.10-0.25 MPa dermis [21], 1 MPa tendon [22], 1.1 MPa ligament [23], 2.6 MPa articular cartilage [24], 0.2-0.76 GPa bone [25], whilst TCP has elastic modulus of ~3 GPa [26]). It is therefore imperative to develop substrates with physiological tissue elasticity to enable the development of functional cell therapies.

In this study, six polyester films with variable elasticity (i.e. from soft to stiff) were fabricated and physicochemically (e.g. nuclear magnetic resonance, Fourier-transform infrared spectroscopy, differential scanning calorimetry, contact angle, surface roughness, mechanical properties, degradation profile) and biologically (e.g. cytocompatibility analysis with human dermal fibroblasts and inflammatory response analysis with a human monocytic cell line) characterised.

2. Materials and methods

2.1. Materials

The aliphatic polyesters used were poly(glycolide-co-ε-caprolactone) (PGCL), poly(glycolide-co-lactide-co-ε-caprolactone-co-trimethylene carbonate) (PGLCLTMC), poly(glycolide-co-dioxanone-co-trimethylene carbonate) (PGDTMC), poly(lactide-co-trimethylene carbonate) (PLTMC) and poly(glycolide-lactide) (PGL) and were produced by Medtronic (North Haven, USA) (Supplementary Fig. S1A). All tissue culture plastics were purchased from Sarstedt (Ireland). All chemicals, cell culture media and reagents were purchased from Sigma Aldrich (Ireland), unless otherwise stated.

2.2. Processing of polymeric films

The polymeric films were obtained by compression moulding, using a thermal presser Carver 3856 CE (Carver, USA). First, the presser was heated close to the polymer melting temperature (PGCL 10/90: 90 °C, PGLCLTMC 70/5/15/10: 175 °C, PGDTMC 55/15/30: 220 °C, PLTMC 80/20: 220 °C, PGL 15/85: 180 °C and PGL 30/70: 220 °C). The polymer pellets were placed between two Teflon sheets and two metal sheets for 5 min and subjected to a minimum pressure of 1 bar. Subsequently the system was gradually cooled down (10 °C/min) to approximately 30 °C. The fabrication method was performed under controlled temperature and humidity conditions. Settings were selected to obtain polymeric films of 200 µm in thickness. Until analysis, samples were stored inside sealed aluminium bags in desiccants at 4 °C.

2.3. Nuclear magnetic resonance (NMR) analysis

Samples for NMR analysis were prepared by dissolving the polymers in deuterated trifluoroacetic acid. A quantitative 13C NMR Spectroscopy with Inverse Gated 1H-Decoupling was utilised that is an 1D-sequence with inverse gated decoupling using a 90 ° pulse. The calculations made as molar ratios based on the relative integral area specific for each polymer region.

2.4. Fourier-transform infrared spectroscopy (FTIR) analysis

FTIR measurements were obtained using the attenuated total reflection technique with a Spectrum 100 FT-IR Spectrometer (Perkin Elmer, USA) by averaging 32 scans over the range of 4,000 cm^{-1} to 800 cm^{-1}.

2.5. Gel permeation chromatography (GPC) analysis

The GPC system was a Waters Alliance GPC 2000 chromatography system (Agilent Technologies, USA) equipped with a differential refractive index detector. The mobile phase was hexafluoroisopropanol (0.3 ml/min) at 40 °C. Polymers were dissolved in hexafluoroisopropanol (1 mg/ml) and measured with a flow rate of 0.3 ml/min at 40 °C. Polydispersity index (PDI) was calculated as the ratio of the weight average molecular weight (M_w) to number average (M_n). PDI is an indicator of the homogeneity of the polymer chains and values of < 2 are indicative of a fairly homogeneous polymer population [27].

2.6. Differential scanning calorimetry (DSC) analysis

The DSC equipment (DSC 1 Star System, Mettler Toledo, USA) was programmed to perform two heating cycles, with a cooling intermediated step. The following temperatures heating protocols were used for each polymer: PGCL 10/90: -75°C to 75°C, PGLCLTMC 70/5/15/10: 0°C to 200°C, PGDTMC 55/15/30: -10 °C to 225 °C, PLTMC 80/20: 30°C to 190°C, PGL 15/85: 30°C to 180°C and PGL 30/70: 30°C to 250°C. All tests were performed at a heating rate of 10 °C/min. The mass of the analysed sample was between 5 and 6 mg. The second heating cycle was used to determine the glass transition temperature (T_g), enthalpy of cold crystallization (ΔH_{cc}), melting temperature (T_m), enthalpy of melting (ΔH_m) and crystallinity content X_c. The crystallinity percentage X_c of the polyesters was determined by the following formula [28] $X_c = [(\Delta H_m - \Delta H_{cc}) / (\Delta H_{mc} w)] \times 100$, where ΔH_m is the melting enthalpy (J/g) of the sample, ΔH_{cc} is the cold crystallization enthalpy (J/g), ΔH_{mc} is the melting enthalpy of the 100 % crystalline poly(lactide) (93.7 J/g) [28], poly(ε-caprolactone) (136.1 J/g) [29], poly(glycolide) (183.2 J/g) [30] and w is the mass fraction of predominant polymer in the composite.

2.7. Contact angle analysis

Static contact angle measurements were obtained using the sessile drop method and an OCA 15 Plus goniometer (DataPhysics In-

* Corresponding author.
E-mail address: dimitrios.zeugolis@usi.ch (D.I. Zeugolis).

struments, Germany) with a high-performance image processing system (DataPhysics Instruments, Germany). 3 µl of either deionized water or diiodomethane were added using a motor driven syringe at room temperature (RT). The values of surface free energy were calculated by the Owens, Wendt, Rabel and Kaelble (OWRK) method [31] that discerns polar and dispersive components of the surface energy, by using the SCA20 version 2 software (DataPhysics Instruments, Germany). At least six measurements of each condition were performed per group.

2.8. Surface roughness analysis

Surface roughness was analysed using Atomic Force Microscopy (AFM) Dimension Icon (Bruker, USA) in PeakForce Tapping (ScanAsyst, Bruker, USA) mode in air. AFM cantilevers (ScanAsyst-Air, Bruker, USA) made of silicon nitride with a spring constant of 0.4 N/m and frequency of 70 kHz were used. The images, with a scan size of 15 × 15 μm^2, were analysed using a commercial AFM software (Bruker, USA) and the surface roughness was measured as the root mean square (RMS) roughness. RMS was calculated using the Z-sensor height signal. A total of 18 locations (6 locations of 3 replicates) were analysed per formulation.

2.9. Dynamic mechanical analysis (DMA)

The viscoelastic measurements were performed using a DMA Q800 (TA Instruments, USA). The measurements were carried out at 25 °C in dry conditions and 37 °C in wet and dry conditions. Samples were cut in rectangular shapes (approximately 14.5 mm length, 5.3 mm width and 0.2 mm thickness). The geometry of the samples was measured and the samples were clamped in the DMA apparatus. The sample was deformed at constant stress-amplitude (25 µm) over 3 different frequencies (0.1, 1 and 10 Hz) for dry conditions and 1 frequency (1 Hz) for wet conditions.

2.10. Tensile test analysis

Mechanical properties were assessed under uniaxial tension, using a Z005 Zwick/Roell testing machine (UK), loaded with a 10 N load cell [32]. The samples were pre-cut into a dog-bone shape, as per ASTM D882-2010 guidelines. Prior to testing, all samples were incubated overnight at RT in phosphate buffered saline (PBS). Prior to testing, tissue paper was used to remove excess of PBS. The samples thickness was measured using digital calliper (Scienceware, Digi-Max, Sigma-Aldrich, Ireland). Scaffolds that broke at contact points with the grips were rejected from the analysis. The extension rate was set at 5 mm/min. Young's modulus was determined by calculating the slope of the linear portion of the stress-strain curve, the ultimate tensile strength was calculated by using the maximum value of engineering stress, the toughness was calculated using the area under stress-strain curves and strain at break or strain at maximum load are defined as the increase in the films length at failure or at maximum load, respectively, divided by the original length.

2.11. Nanoindentation and force mapping analysis

Experiments were conducted using an AFM (JPK NanoWizard 3, Germany) mounted on a Zeiss inverted microscope (Germany), operating in contact mode. Silicon nitride cantilevers (MSNL, Bruker, Germany) were used for the force mapping measurements. All the cantilevers were calibrated by the contact-based method under PBS at 37 °C, from which it was extracted their respective sensitivity and spring constant (typically between 0.3-1.4 N/m). Samples were fixed in Petri dishes and incubated with PBS at 37 °C overnight prior to the measurements. Force-distance curves were collected using maps with dimensions of 10 µm x 10 µm and arrays of 8 × 8 curves. For each sample, the force maps were repeated 3 times at different positions. All the force distance curves were acquired using a Z-length of 3 µm, a force setpoint of 1 nN and a cantilever approach and retract speed of 3 µm/sec. The JPK data processing (JPK, Germany) was used to analyse the acquired data. The Young's modulus of each sample was determined from the acquired force curves using the Hertz-Sneddon model with the following parameters: quadratic pyramid tip shape, a half-angle face of 15 ° and a Poisson ratio of 0.5. The fitting was executed up to an indentation of 500 nm.

2.12. Degradation profile analysis

Films were incubated in PBS with neutral pH up to 21 days. The pH of the supernatant was measured at each time point and the films were subsequently analysed by DSC, NMR, GPC and tensile tests. The effect of degradation was measured as percentage of decrease or increase in relation to the original value, using the following formula Degradation (%) = [(Final Degradation - Original Degradation) / Original Degradation] x 100.

2.13. Human dermal fibroblasts (hDFs) cultures

Cytocompatibility assessment was conducted using hDFs (American Type Culture Collection, UK). hDFs were expanded in Dulbecco's Modified Eagle Medium (DMEM) supplemented with 10 % foetal bovine serum (FBS) and 1 % penicillin streptomycin (P/S). Cells were cultured at 37 °C in a 95 % air / 5 % CO_2 humidified atmosphere. Confluent hDFs at passage 2-3 were harvested from monolayer cultures using trypsin. Cells were washed in PBS and centrifuged at 1,200 rpm for 10 min. The cell pellet was resuspended in DMEM and seeded at a concentration of 10,000 cells/ml onto the respective polymeric films, which were placed into wells of a 24 well plate. The medium was changed every other day. Cells seeded on TCP served as control group.

2.14. Cell viability analysis

After 3, 5 and 7 days of culture, Live/Dead® assay (Invitrogen, Ireland) was performed to assess the influence of substrate stiffness on hDF viability as per manufacture's protocol. Briefly, cells were washed with HBSS and a solution of calcein AM (4 μM) and ethidium homodimer I (2 μM) was added to each well. Cells were incubated at 37 °C and 5 % CO_2 for 30 min after which, fluorescence images were obtained with an Olympus IX-81 inverted fluorescence microscope (Olympus Corporation, Japan).

2.15. Cytoskeleton and nuclei staining

After 1 and 2 (THP-1 cultures) and 3, 5 and 7 (hDF cultures) days, cells were fixed with 4 % paraformaldehyde (PFA) for 2 h at 4 °C, blocked with 3 % bovine serum albumin (BSA) in PBS for 30 min at RT and permeabilised with 0.2 % Triton X-100 for 5 min at RT. After 3 washes with PBS, the samples were incubated in rhodamine labelled phalloidin (1:200, Invitrogen, Ireland) for 2 h at RT to stain cytoskeleton and the nuclei were stained with Hoechst 33342 Solution (1:5000, Invitrogen, Ireland) for 5 min at RT. Fluorescent images were captured using an Olympus IX-81 inverted fluorescence microscope (Olympus Corporation, Japan) at 10x magnification.

2.16. Cell proliferation analysis

After 1 and 2 (THP-1 cultures) and 3, 5 and 7 (hDF cultures) days, cell proliferation was assessed through stained nuclei counting with ImageJ (NIH, USA). Three substrates were imaged and four

fields-of-view (FOV) were taken from each substrate (total of 12 images were analysed per experimental group).

2.17. Cell metabolic activity analysis

After 1 and 2 (THP-1 cultures) and 3, 5 and 7 (hDF cultures) days, alamarBlue™ assay (Invitrogen, USA) was used to quantify the metabolic activity of the cells according to the manufacturer's protocol. At the end of each timepoint, cells were washed with Hanks' Balanced Salt solution (HBSS, Sigma Aldrich, Ireland) and alamarBlue™ solution (10 % alamarBlue™ in HBSS) was added. After 4 h of incubation at 37°C, absorbance was measured in triplicate at 550 nm and 595 nm using Varioskan Flash spectral scanning multimode reader (Thermo Scientific, UK). Cell metabolic activity was normalised by DNA content.

2.18. DNA quantification

After 1 and 2 (THP-1 cultures) and 3, 5 and 7 (hDF cultures) days, DNA was quantified using Quant-iT™ PicoGreen® dSDNA assay kit (Invitrogen, Ireland) according to the manufacturer's protocol. Briefly, DNA was extracted using three freeze-thaw cycles after adding 250 μl of nucleic acid free water per well. 100 µl of sample were transferred into a 96-well plate. A standard curve was generated using 0, 5, 10, 25, 50, 100, 500 and 1,000 ng/ml DNA concentrations. 100 µl of a 1:200 dilution of Quant-iT™ PicoGreen® reagent was added to each sample and the plate was read using a micro-plate reader (Varioskan Flash, Thermo Scientific, UK) with an excitation wavelength of 480 nm and an emission wavelength of 525 nm.

2.19. THP-1 cultures and analysis

Immune response was assessed as has been described previously [33,34]. Monocyte-like cells (THP-1, ATCC, UK) were expanded in RPMI-1640 medium supplemented with 10 % FBS and 1 % P/S and seeded with a concentration of 25,000 cells/cm^2. Indirect cell cytotoxicity was assessed incubate the polymeric samples in RPMI medium with 10 % FBS and 1 % P/S for three days. Subsequently, the conditioned media (CM) was placed in contact with cells seeded on TCP. For direct cell cytotoxicity assessment, cells were seeded on the polymeric films. To induce macrophage phenotype, cells were treated with phorbol 12-myristate 13-acetate (PMA, P8139, Sigma-Aldrich, Ireland) at 100 ng/ml for 6 h. Non-attached cells were washed with PBS. As positive control, cells were treated with 100 ng/ml lipopolysaccharides (LPS) from *E. Coli* (L2637, Sigma-Aldrich, Ireland) to induce inflammatory response. To assess the immune response *in vitro*, cell morphology was analysed after rhodamine-phalloidin/Hoechst staining and imaging. Images were analysed with ImageJ (NIH, USA) and the circularity was measured. The relative number of elongated cells was calculated by classifying those cells with a circularity superior to 0.5 as round cells, whilst cells with circularity inferior to 0.5 were considered as elongated. The formation of cell clusters ($\geq$ 5 cells) was also assessed.

2.20. Statistical analysis

Data are expressed as mean ± standard deviation. All experiments were conducted at least in three independent replicates. Statistical analysis was performed using GraphPad v6.01 (GraphPad Software Inc., USA). One- or two- way ANOVA was used for multiple comparisons and a Tukey *post hoc* test was used for pairwise comparisons after confirming that the samples followed a normal distribution (Kolmogorov-Smirnov test) and had equal variances (Bartlett's and Levene's test for homogeneity of variances). When either or both of these assumptions were violated, nonparametric tests were used for multiple comparisons (Kruskal-Wallis test) and pairwise comparisons (Mann-Whitney test). Statistical significance was accepted at $p < 0.05$.

3. Results

3.1. Chemical, thermal, wettability and roughness analysis

The values of the determined composition ratios of the polymeric samples obtained from NMR spectra analysis (Supplementary Fig. S2) are provided in Table 1. The M_w and PDI of the studied polymeric films are provided in Table 2. The PLTMC 80/20 showed the lowest ($p < 0.001$) PDI, whilst the PGCL 10/90 showed the highest PDI ($p < 0.001$). Moreover, the PLTMC 80/20 had the highest ($p < 0.001$) M_w and M_n, whilst the PGLCLTMC 70/5/15/10 showed the lowest ($p < 0.001$) M_w and M_n.

The spectra obtained by FTIR for the polymeric films are presented in Supplementary Fig. S1B. All the spectra had strong bands in the region between 1,760 and 1,750 cm^{-1}, due to stretch of the carbonyl groups present in the five polymers. Stretching bands, due to asymmetric and symmetric C-C(=O)-O vibrations between 1,300 and 1,150 cm^{-1}, were also detected.

DSC was performed to assess the materials thermal properties. Supplementary Fig. S3 shows the DSC curves for the second heating in the thermal study of the pellets and the polymeric films. The thermal properties of the materials are summarised in Table 3. The PGCL 10/90 pellet and film exhibited the lowest ($p < 0.001$) T_g and the PGL 15/85 pellet and film exhibited the highest ($p < 0.001$) T_g. The PGCL 10/90 pellet and film exhibited the lowest ($p < 0.001$) T_m and the PLTMC 80/20 pellet and film exhibited the highest ($p < 0.001$) T_m. The PGCL 10/90 pellet and film exhibited the highest ($p < 0.001$) ΔH_m and the PLTMC 80/20 and the PGLCLTMC 70/5/15/10, exhibited the lowest ($p < 0.001$), pellet and film, respectively, ΔH_m. The PGCL 10/90 pellet and film exhibited the highest ($p < 0.001$) X_c and the PLTMC 80/20 and the PGLCLTMC 70/5/15/10 exhibited the lowest ($p < 0.001$) pellet and film, respectively, X_c. T_m, ΔH_m and X_c were not detected for PGL 15/85 and PGL 30/70.

The sessile drop method was used to assess the contact angle of the samples and the measurements are presented in Table 4. The water contact angles were the highest ($p < 0.001$) for the PLTMC 80/20 and the lowest ($p < 0.001$) for PGLCLTMC 70/5/15/10. With diiodomethane, the highest ($p < 0.001$) contact angles were obtained for the PGDTMC 55/15/30 and lowest ($p < 0.001$) contact angles were obtained for the PGLCLTMC 70/5/15/10. The highest ($p < 0.001$) surface energy values were recorded for the PGLCLTMC 70/5/15/10 and the lowest ($p < 0.001$) for the PGDTMC 55/15/30. The highest ($p < 0.001$) dispersive components values were obtained for the PGLCLTMC 70/5/15/10 and lowest ($p < 0.001$) for the PGDTMC 55/15/30. The highest ($p < 0.001$) polar component values were obtained for the PGL 15/85 and lowest ($p < 0.001$) for the PLTMC 80/20 and the PGCL 10/90.

AFM analysis made apparent that all formulations had a similar ($p > 0.05$) RMS roughness (Supplementary Table S1) and appearance (Supplementary Figure S4) over a square 15 µm scan size.

3.2. Mechanical analysis

DMA at 25 °C and under dry conditions (Table 5) revealed that the PGL 30/70 exhibited the highest ($p < 0.001$) and the PGCL 10/90 the lowest ($p < 0.001$) storage moduli for all frequencies. Under the same conditions, the PGLCLTMC 70/5/15/10 had the highest ($p < 0.001$) and the PGCL 10/90 had the lowest ($p < 0.001$) loss modulus for all frequencies. For both storage and

Table 1
Determined composition of polymers via NMR without degradation and after 21 days of degradation. The effect of degradation was measured as % of decrease or increase at a given degradation timepoint in relation to a sample's original value (without degradation). Red font indicates the highest reduction. N = 3.

Material		% Glycolide (G)	% Caprolactone (CL)	% Lactide (L)	% Trimethylene carbonate (TMC)	% Dioxanone (D)	DSC Heating
PGCL 10/90	Film	9.6	90.4	0.0	0.0	0.0	-75°C to 75°C
PGLCLTMC 70/5/15/10		70.5	16.6	5.0	7.9	0.0	0°C to 200°C
PGDTMC 55/15/30		56.8	0.0	0.0	27.7	15.5	-10 °C to 225 °C
PLTMC 80/20		0.0	0.0	79.1	20.9	0.0	30°C to 190°C
PGL 15/85		18.1	0.0	81.9	0.0	0.0	30°C to 180°C
PGL 30/70		31.4	0.0	68.6	0.0	0.0	30°C to 250°C
PGCL 10/90	21 days	9.8 (2 %)	90.2 (0 %)	0.0 (ND)	0.0 (ND)	0.0 (ND)	-75°C to 75°C
PGLCLTMC 70/5/15/10		68.2 (-3 %)	18.1 (9 %)	5.2 (5 %)	8.5 (7 %)	0.0 (ND)	0°C to 200°C
PGDTMC 55/15/30		56.0 (-2 %)	0.0 (ND)	0.0 (ND)	27.5 (-1 %)	16.5 (7 %)	-10 °C to 225 °C
PLTMC 80/20		0.0 (ND)	0.0 (ND)	79.0 (0 %)	21.0 (0 %)	0.0 (ND)	30°C to 190°C
PGL 15/85		18.0 (-1 %)	0.0 (ND)	82.0 (0 %)	0.0 (ND)	0.0 (ND)	30°C to 180°C
PGL 30/70		41.2 (31 %)	0.0 (ND)	58.8 (-14 %)	0.0 (ND)	0.0 (ND)	30°C to 250°C

Table 2
Polydispersity (PDI), number-average molecular weight (M_n), weight-average molecular weight (M_w) determined by gel permeation chromatography (GPC) with hexafluoroisopropanol before and after degradation. The effect of degradation was measured as % of decrease or increase at a given degradation timepoint in relation to a sample's original value (without degradation). Green font indicates the highest ($p < 0.001$) value and red font indicates the lowest ($p < 0.001$) value. N=3.

Material		PDI (M_w/M_n)	M_n (kg/mol)	M_w (kg/mol)
PGCL 10/90	Film	2.9 ± 0.1	47 ± 2	138 ± 0
PGLCLTMC 70/5/15/10		2.6 ± 0.1	27 ± 1	69 ± 1
PGDTMC 55/15/30		2.3 ± 0.1	42 ± 1	98 ± 1
PLTMC 80/20		1.5 ± 0	120 ± 2	184 ± 4
PGL 15/85		2.3 ± 0.1	56 ± 2	127 ± 1
PGL 30/70		2.3 ± 0.1	41 ± 1	95 ± 2
PGCL 10/90	21 days	2.7 ± 0.1 (-6 %)	46 ± 1 (-3 %)	125 ± 2 (-9 %)
PGLCLTMC 70/5/15/10		1.2 ± 0 (-54 %)	4 ± 0 (-86 %)	4 ± 0 (-94 %)
PGDTMC 55/15/30		1.3 ± 0 (-43 %)	9 ± 0 (-79 %)	12 ± 0 (-88 %)
PLTMC 80/20		1.4 ± 0 (-11 %)	112 ± 1 (-7 %)	152 ± 1 (-17 %)
PGL 15/85		2.0 ± 0 (-13 %)	39 ± 1 (-31 %)	77 ± 0 (-40 %)
PGL 30/70		2.4 ± 0 (1 %)	12 ± 0 (-70 %)	29 ± 0 (-70 %)

Table 3
Thermal properties of the second heating curve of pellets and polymeric films produced in this study without degradation and after 14 and 21 days of degradation. Red font indicates the lowest ($p < 0.001$) and green font indicates the highest ($p < 0.001$) values within a group (without degradation, after 14 days of degradation and after 21 days of degradation). The effect of degradation was measured as % of decrease or increase at a given degradation timepoint in relation to a sample's original value (without degradation). T_g: glass transition temperature, ΔH_{cc}: enthalpy of cold crystallization, T_m: melting temperature, ΔH_m: enthalpy of melting, X_c: and crystallinity content, ND: not detected. N = 4.

Material		T_g (°C)	ΔH_{cc} (J/g)	T_m (°C)	ΔH_m (J/g)	X_c
PGCL 10/90	Pellet	-57 ± 0	ND	30 ± 0	40 ± 1	9.2 ± 0.4
PGLCLTMC 70/5/15/10		25 ± 1	ND	99 ± 1	24 ± 2	4.0 ± 1.0
PGDTMC 55/15/30		4 ± 1	ND	147 ± 0	22 ± 0	4.1 ± 0.6
PLTMC 80/20		54 ± 1	10 ± 2	164 ± 1	14 ± 1	1.0 ± 0.2
PGL 15/85		61 ± 0	ND	ND	ND	ND
PGL 30/70		57 ± 2	ND	ND	ND	ND
PGCL 10/90	Film	-52 ± 1	ND	31 ± 1	46 ± 2	10.0 ± 1.0
PGLCLTMC 70/5/15/10		22 ± 1	ND	114 ± 1	18 ± 1	2.1 ± 0.0
PGDTMC 55/15/30		14 ± 2	ND	163 ± 2	32 ± 2	5 ± 1
PLTMC 80/20		51 ± 0	30 ± 2	166 ± 0	40 ± 1	3 ± 1
PGL 15/85		61 ± 1	ND	ND	ND	ND
PGL 30/70		56 ± 1	ND	ND	ND	ND
PGCL 10/90	14 days	-51 ± 0 (1 %)	ND	31 ± 0 (-6 %)	40 ± 1 (-12 %)	8 ± 1 (-24 %)
PGLCLTMC 70/5/15/10	degradation	11 ± 7 (-51 %)	ND	115 ± 0 (1 %)	24 ± 1 (35 %)	5 ± 0 (132 %)
PGDTMC 55/15/30		17 ± 2 (15 %)	ND	159 ± 0 (-3 %)	33 ± 4 (5 %)	10 ± 3 (86 %)
PLTMC 80/20		50 ± 2 (-3 %)	27 ± 1 (-10 %)	164 ± 2 (-2 %)	40 ± 1 (0 %)	5 ± 1 (49 %)
PGL 15/85		61± 1 (1 %)	ND	ND	ND	ND
PGL 30/70		55 ± 0 (-2 %)	3 ± 1 (ND)	191 ± 3 (ND)	8 ± 1 (ND)	2 ± 0 (ND)
PGCL 10/90	21 days	-56 ± 1 (-7 %)	ND	30 ± 2 (-6 %)	44 ± 1 (-3 %)	9 ± 1 (-13 %)
PGLCLTMC 70/5/15/10	degradation	7 ± 0 (-70 %)	ND	109 ± 0 (-4 %)	28 ± 3 (59 %)	6 ± 1 (168 %)
PGDTMC 55/15/30		16 ± 2 (13 %)	ND	157 ± 2 (-4 %)	36 ± 0 (15 %)	6 ± 1 (7 %)
PLTMC 80/20		51 ± 0 (0 %)	30 ± 2 (-1 %)	165 ± 1 (-1 %)	42 ± 1 (4 %)	4 ± 1 (8 %)
PGL 15/85		61 ± 0 (-14 %)	ND	ND	ND	ND
PGL 30/70		55 ± 0 (-1 %)	3 ± 1 (ND)	187 ± 4 (ND)	8 ± 2 (ND)	2 ± 0 (ND)

Table 4
Contact angles and surface energy of the polymeric films produced in this study. Red font indicates the lowest ($p < 0.001$) and green font indicates the highest ($p < 0.001$) values within a group. N = 4.

Material	Contact angle (°)		Surface Energy (mN/m)		
	Water	Diiodomethane	Surface Energy	Dispersive component	Polar Component
PGCL 10/90	86 ± 4	37 ± 5	39 ± 0	36 ± 0	3 ± 0
PGLCLTMC 70/5/15/10	81 ± 1	31 ± 0	43 ± 0	40 ± 0	4 ± 0
PGDTMC 55/15/30	86 ± 4	71 ± 2	25 ± 0	17 ± 0	8 ± 0
PLTMC 80/20	95 ± 4	56 ± 1	29 ± 0	27 ± 0	2 ± 0
PGL 15/85	85 ± 3	64 ± 2	28 ± 0	20 ± 0	8 ± 0
PGL 30/70	85 ± 4	59 ± 6	30 ± 0	24 ± 0	5 ± 0

Table 5
Storage and loss modulus of the polymeric films produced in this study under dry conditions at 25 °C and 37 °C as a function of frequency. Red font indicates the lowest ($p < 0.001$) and green font indicates the highest ($p < 0.001$) values within a group. N = 4.

Material	25 °C						37 °C					
	Storage modulus (MPa)			Loss modulus (MPa)			Storage modulus (MPa)			Loss modulus (MPa)		
	1 Hz	5 Hz	10 Hz	1 Hz	5 Hz	10 Hz	1 Hz	5 Hz	10 Hz	1 Hz	5 Hz	10 Hz
PGCL 10/90	179 ± 1	187 ± 1	190 ± 1	10 ± 1	9 ± 0	9 ± 0	143 ± 4	149 ± 4	152 ± 4	9 ± 0	9 ± 1	8 ± 1
PGLCLTMC 70/5/15/10	776 ± 26	1022 ± 36	1149 ± 38	240 ± 9	328 ± 9	363 ± 9	442 ± 24	541 ± 34	593 ± 37	93 ± 11	141 ± 15	167 ± 15
PGDTMC 55/15/30	488 ± 8	570 ± 9	619 ± 10	73 ± 2	111 ± 3	135 ± 4	407 ± 4	447 ± 6	469 ± 6	38 ± 57	57 ± 2	68 ± 3
PLTMC 80/20	2,390 ± 8	2,452 ± 8	2,480 ± 8	112 ± 1	113 ± 0	117 ± 1	2,267 ± 9	2,332 ± 9	2,357 ± 10	117 ± 2	117 ± 1	120 ± 1
PGL 15/85	2,984 ± 3	3,006 ± 2	3,019 ± 3	120 ± 0	124 ± 1	130 ± 0	2,926 ± 5	2,946 ± 4	2,957 ± 4	125 ± 1	125 ± 1	131 ± 1
PGL 30/70	3,753 ± 4	3,783 ± 4	3,798 ± 5	144 ± 1	147 ± 1	152 ± 1	3,673 ± 7	3,706 ± 8	3,720 ± 8	149 ± 1	147 ± 1	151 ± 1

Table 6
Storage and loss modulus of the polymeric films produced in this study under dry and wet conditions at 1 Hz frequency and 37 °C. Red font indicates the lowest ($p < 0.001$) and green font indicates the highest ($p < 0.001$) values within a group. N = 4.

Material	Dry		Wet	
	Storage modulus (MPa)	Loss modulus (MPa)	Storage modulus (MPa)	Loss modulus (MPa)
PGCL 10/90	143 ± 4	9 ± 0	108 ± 4	9 ± 0
PGLCLTMC 70/5/15/10	442 ± 24	93 ± 11	272 ± 3	21 ± 0
PGDTMC 55/15/30	407 ± 4	38 ± 1	321 ± 5	15 ± 1
PLTMC 80/20	2,267 ± 9	117 ± 2	1,385 ± 60	249 ± 14
PGL 15/85	2,926 ± 5	125 ± 1	2,756 ± 156	227 ± 49
PGL 30/70	3,673 ± 7	149 ± 1	947 ± 116	507 ± 8

loss moduli at 25 °C under dry conditions, there were no significant ($p > 0.05$) differences between 1, 5 and 10 Hz frequencies for PGCL 10/90, PLTMC 80/20, PGL 15/85 and PGL 70/30, whilst PGLCLTMC 70/5/15/10 and PGDTMC 55/15/30 showed significant ($p < 0.001$) increase of the storage and loss moduli by increasing the frequency.

DMA at 37 °C and under dry conditions (Table 5) made apparent that the PGL 30/70 had the highest ($p < 0.001$) and the PGCL 10/90 had the lowest ($p < 0.001$) storage moduli across all frequencies. Under the same conditions, the PGL 30/70 at all frequencies and PGLCLTMC 70/5/15/10 only at 10 Hz frequency had the highest ($p < 0.001$) loss modulus and the PGCL 10/90 had the lowest ($p < 0.001$) loss modulus across all frequencies. For both storage and loss moduli at 37 °C under dry conditions, there were no significant ($p > 0.05$) differences between 1, 5 and 10 Hz frequencies for PGCL 10/90, PLTMC 80/20, PGL 15/85 and PGL 70/30, whilst PGLCLTMC 70/5/15/10 showed significant ($p < 0.001$) increase of the storage and loss moduli by increasing the frequency. PGDTMC 55/15/30 showed significant ($p < 0.001$) increase in storage modulus between 1 and 10 Hz frequency and loss modulus was significantly ($p < 0.001$) increased with increasing the frequency.

DMA at 37 °C, 1 Hz frequency and in dry state (Table 6) revealed that the PGL 30/70 exhibited the highest ($p < 0.001$) and the PGCL 10/90 exhibited the lowest ($p < 0.001$) for both storage and loss moduli. DMA at 37 °C, 1 Hz frequency and in wet state (Table 6) revealed that the PGL 15/85 and the PGL 30/70 exhibited the highest ($p < 0.001$) storage and loss moduli, respectively, and the PGCL 10/90 exhibited the lowest ($p < 0.001$) storage and loss moduli.

Tensile test analysis (Table 7) made apparent that the PGL 30/70 exhibited the highest ($p < 0.001$) Young's modulus, ultimate tensile strength and toughness. The PGCL 10/90, PGLCLTMC 70/5/15/10 and PGDTMC 55/15/30 exhibited significantly ($p < 0.001$) lower Young's modulus than PLTMC 80/20, PGL 15/85 and PGL 30/70. PGCL 10/90 exhibited the lowest ($p < 0.001$) ultimate tensile strength and toughness values. The PGLCLTMC 70/5/15/10 exhibited the highest ($p < 0.001$) and PGL 15/85 the lowest ($p < 0.001$) strain at break. Stress-strain curves (Supplementary Fig. S5A) revealed that the PGCL 10/90, PGLCLTMC 70/5/15/10 and PGDTMC 55/15/30 had curves with a slowly rising stress (up to 10-20 % strain) followed by a long region of constant gradient up to the point of break (over 60 % strain), whilst the PLTMC 80/20, PGL 15/85 and PGL 30/70 (also exhibited a toe region up to 0.03 % strain) had curves with steeply rising stress, at the end of which (2-5 % strain) break occurred.

AFM analysis (Table 7) revealed that the PGL 30/70 exhibited the highest ($p < 0.001$) Young's modulus (~15 MPa), whilst all other materials had Young's modulus in the region of ~6 (PGLCLTMC 70/5/15/10) to ~22 (PGL 15/85) kPa.

3.3. Degradation profile analysis

Degradation profile analysis (Supplementary Fig. S6) made apparent that TCP and PGCL 10/90, PGL 15/85 and PLTMC 80/20 had

Table 7
Macro-scale Young's modulus, ultimate tensile strength, toughness and strain at break (or tensile strain at maximum load, indicated with *); all assessed via tensile test analysis] and nano-scale (Young's modulus; assessed via AFM) mechanical properties of the polymeric films produced in this study without degradation and after 7, 11, 14 and 21 days of degradation. Red font indicates the lowest ($p < 0.001$) and green font indicates the highest ($p < 0.001$) values within a group (without degradation, after 7 days of degradation, after 11 days of degradation, after 14 days of degradation and after 21 days of degradation). The effect of degradation was measured as % of decrease or increase at a given degradation timepoint in relation to a sample's original value (without degradation). ND: not detected. NA: not available. N = 4.

Material		Tensile Analysis				AFM Analysis
		Young's Modulus (MPa)	Ultimate Tensile Strength (MPa)	Toughness (MJ/m^3)	Strain at Break (%)	Young's Modulus (kPa)
PGCL 10/90	Original	110 ± 8	8 ± 2	23 ± 1	168 ± 3*	7 ± 3
PGLCLTMC 70/5/15/10		114 ± 17	18 ± 2	39 ± 4	278 ± 85*	6 ± 2
PGDTMC 55/15/30		111 ± 14	30 ± 4	39 ± 2	223 ± 75*	10 ± 3
PLTMC 80/20		1,288 ± 22	47 ± 1	221 ± 12	5 ± 0	12 ± 3
PGL 15/85		1,601 ± 121	37 ± 3	143 ± 23	3 ± 0	22 ± 9
PGL 30/70		2,184 ± 132	62 ± 5	287 ± 12	4 ± 0	15,019 ± 2,916
PGCL 10/90	7 days degradation	124 ± 5 (12 %)	8 ± 0 (2 %)	10 ± 0 (-56 %)	160 ± 1* (-1 %)	NA
PGLCLTMC 70/5/15/10		153 ± 46 (34 %)	14 ± 2 (-24 %)	16 ± 1 (-60 %)	199± 3* (-29 %)	
PGDTMC 55/15/30		173 ± 29 (56 %)	23 ± 3 (-25 %)	16 ± 3 (-60 %)	155 ± 4* (-30 %)	
PLTMC 80/20		989 ± 81 (-23 %)	29 ± 3 (-38 %)	61 ± 3 (-73 %)	4 ± 1 (-13 %)	
PGL 15/85		1,448 ± 74 (-10 %)	49 ± 4 (34 %)	93 ± 9 (-35 %)	4 ± 1 (32 %)	
PGL 30/70		1,075 ± 235 (-51 %)	23 ±6 (-62 %)	29 ± 10 (-90 %)	2 ± 0 (-49 %)	
PGCL 10/90	11 days	123 ± 6 (13 %)	8 ± 1 (2 %)	10 ± 1 (-56 %)	160 ± 3* (-5 %)	
PGLCLTMC 70/5/15/10	degradation	221 ± 69 (93 %)	1 ± 0 (-94 %)	1 ± 0 (-98 %)	0.3 ± 0 (-100 %)	
PGDTMC 55/15/30		222 ± 9 (99 %)	12 ± 1 (-61 %)	14 ± 2 (-63 %)	7 ± 1 (-97 %)	
PLTMC 80/20		1,097 ± 130 (-15 %)	41 ± 6 (-13 %)	72 ± 2 (-67 %)	4 ± 0 (-6 %)	
PGL 15/85		1,378 ± 216 (-14 %)	46 ± 9 (25 %)	85 ± 21 (-40 %)	4 ± 0 (24 %)	
PGL 30/70		841 ± 176 (-62 %)	7 ± 1 (-81 %)	11 ± 12 (-96 %)	1 ± 0 (-64 %)	
PGCL 10/90	14 days	104 ± 6 (-6 %)	8 ± 1 (2 %)	9 ± 0 (-61 %)	159 ± 14* (-5 %)	
PGLCLTMC 70/5/15/10	degradation	ND	ND	ND	ND	
PGDTMC 55/15/30		ND	ND	ND	ND	
PLTMC 80/20		973 ± 32 (-25 %)	38 ± 2 (-18 %)	64 ± 2 (-71 %)	5 ± 0 (2 %)	
PGL 15/85		899 ± 125 (-44 %)	29 ± 6 (-22 %)	46 ± 16 (-68 %)	3 ± 0 (19 %)	
PGL 30/70		ND	ND	ND	ND	
PGCL 10/90	21 days	124 ± 7 (12 %)	8 ± 1 (4 %)	10 ± 0 (-58 %)	151 ± 3* (-10 %)	
PGLCLTMC 70/5/15/10	degradation	ND	ND	ND	ND	
PGDTMC 55/15/30		ND	ND	ND	ND	
PLTMC 80/20		1,088 ± 73 (-16 %)	41 ± 4 (-12 %)	73 ± 5 (-67 %)	5 ± 1 (10 %)	
PGL 15/85		1,242 ± 170 (-12 %)	37 ± 16 (1 %)	37 ± 2 (-74 %)	3 ± 1 (-3 %)	
PGL 30/70		NA	NA	NA	NA	

no significant ($p > 0.05$) pH changes over the incubation period, whilst the PGLCLTMC 70/5/15/10 and the PGDTMC 55/15/30 and the PGL 30/70 started degrading from day 7 and day 12 onwards, respectively, as evidenced by reduced solution pH.

The values of the determined composition ratios of the degraded polymeric films obtained from NMR spectra analysis (Supplementary Fig. S7) are presented in Table 1 and indicate that the PGL 30/70 suffered the highest degradation, as evidenced by a 14 % reduction in the lactide content.

GPC analysis at 21 days of degradation (Table 2) showed that the PGLCLTMC 70/5/15/10 had the lowest ($p < 0.001$) PDI, M_w and M_n and the lowest ($p < 0.001$) drop on each of these values in comparison to the original film. The PGCL 10/90 exhibited the highest ($p < 0.001$) PDI and the PLTMC 80/20 exhibited the highest ($p < 0.001$) M_w and M_n. The PGL 30/70 exhibited the highest ($p < 0.001$) increase in PDI and the PGCL 10/90 exhibited the highest increase ($p < 0.001$) in M_w and M_n.

DSC analysis following degradation (Table 3) revealed that after 14 and 21 days of degradation the highest ($p < 0.001$) T_g was obtained for the PGL 15/85 and the lowest ($p < 0.001$) for the PGCL 10/90; the highest ($p < 0.001$) drop in T_g, compared to the original film, was obtained for the PGLCLTMC 70/5/15/10 at both timepoints. The highest ($p < 0.001$) ΔH_{cc} was obtained for the PLTMC 80/20 and the lowest ($p < 0.001$) for the PGL 30/70. The highest ($p < 0.001$) T_m was obtained for the PGL 30/70 and the lowest ($p < 0.001$) for the PGCL 10/90; with the highest ($p < 0.001$) drop in T_m, compared to the original film, was obtained for the PGCL 10/90. The highest ($p < 0.001$) ΔH_m was obtained for the PGCL 10/90 and the lowest ($p < 0.001$) for the PGL 30/70, at both timepoints. PGCL 10/90 exhibited the highest ($p < 0.001$) drop in ΔH_m, compared to the original polymeric film. The highest ($p < 0.001$) X_c was obtained for the PGDTMC 55/15/30 at day 14 and the PGCL 10/90 at day 21 and the lowest ($p < 0.001$) for the PGL 30/70 at both timepoints. The highest ($p < 0.001$) drop in X_c, in comparison to the original film, was obtained for the PGCL 10/90 at both timepoints and the highest ($p < 0.001$) increase in X_c, in comparison to the original film, was obtained for the PGLCLTMC 70/5/15/10 at both timepoints. At day 14 and 21, T_m, ΔH_m and X_c were not detected for PGL 15/85.

Tensile analysis following degradation (Table 7) made apparent that at 7 days of degradation, the PGCL 10/90 exhibited the lowest ($p < 0.001$) and the PGL 15/85 the highest ($p < 0.001$) Young's modulus, ultimate tensile strength and toughness values and the PGLCLTMC 70/5/15/10 exhibited the highest ($p < 0.001$) and the PGL 30/70 the lowest ($p < 0.001$) strain at break values. At 11 days of degradation, the PGCL 10/90 and PGLCLTMC 70/5/15/10 exhibited the lowest ($p < 0.001$) Young's modulus values and ultimate tensile strength, toughness and stress at break values, respectively, and the PGL 15/85 and the PLTMC 80/20 exhibited the highest ($p < 0.001$) Young's modulus, ultimate tensile strength and toughness and stress at break values, respectively. At 14 days of degradation, the PGCL 10/90 exhibited the lowest ($p < 0.001$) Young's modulus, ultimate tensile strength and toughness values and the highest ($p < 0.001$) strain at break values, the PLTMC 80/20 exhibited the highest ($p < 0.001$) Young's modulus, ultimate tensile strength and toughness values and the PGL 15/85 the lowest ($p < 0.001$) strain at break values. At 21 days of degradation, the PGCL 10/90 exhibited the lowest ($p < 0.001$) Young's modulus, ultimate tensile strength and toughness values and the highest ($p < 0.001$) strain at break values, the PGL 15/85 exhibited the highest

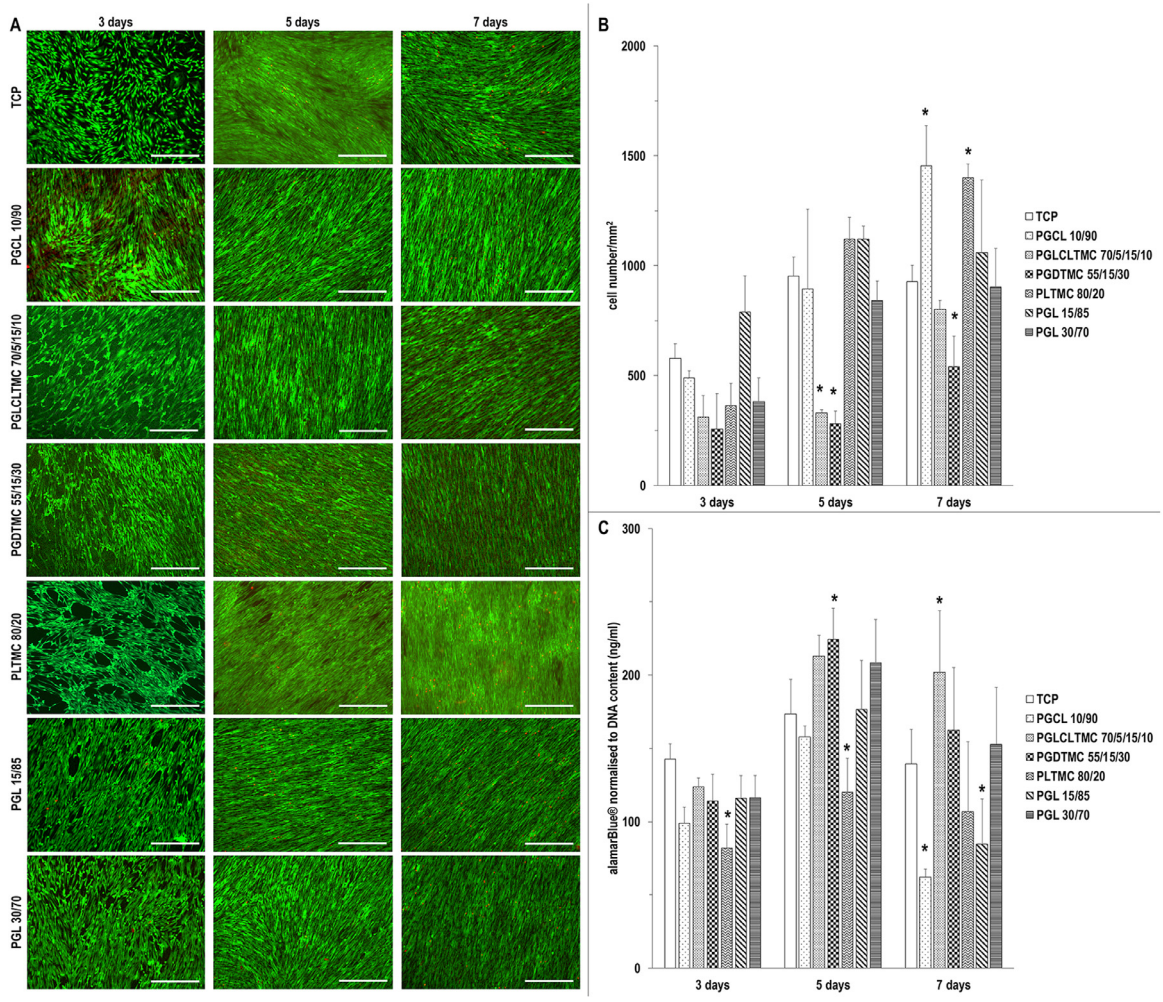

Fig. 1. hDF viability (A) was not affected as a function of the various substrates at any timepoint, as revealed by Live/Dead^{TM} assay; live cells: green, dead cells: red, scale bar: 500 µm. A polymer-dependent hDF proliferation (B) and metabolic activity (C) was observed; * indicates significant difference at $p < 0.001$ between a group and TCP at a given timepoint.

($p < 0.001$) Young's modulus values and the lowest ($p < 0.001$) strain at break values and the PLTMC 80/20 exhibited the highest ($p < 0.001$) toughness and ultimate tensile strength values.

After 7 days of degradation, the PGL 30/70 exhibited the highest ($p < 0.001$) drop, in comparison to the original film, in Young's modulus, ultimate tensile strength, toughness and strain at break. After 11 days of degradation, in comparison to the original film, the PGL 30/70 exhibited the highest ($p < 0.001$) drop in Young's modulus, the PGLCLTMC 70/5/15/10 exhibited the highest ($p < 0.001$) drop in ultimate tensile strength, the PGLCLTMC 70/5/15/10 and the PGL 30/70 exhibited the highest ($p < 0.001$) drop in toughness and the PGLCLTMC 70/5/15/10 and the PGDTMC 55/15/30 exhibited the highest ($p < 0.001$) drop in strain at break. After 14 and 21 days of degradation, the PGLCLTMC 70/5/15/10, PGDTMC 55/15/30 and PGL 30/70 became too brittle to be mechanically assessed.

Stress-stain curve analysis (Supplementary Fig. S5) revealed that all polymers maintained their original deformation mechanism, but with reduced values subject to degradation period, with only the PGCL 10/90 maintaining an unaltered deformation mechanism up to day 21, with the PGL 15/85 and PLTMC 80/20 to follow.

3.4. Biological analysis

Nuclei / cytoskeleton staining (Supplementary Figure S8), viability (Fig. 1A), proliferation (Fig. 1B) and metabolic activity (Fig. 1C) analyses revealed that all substrates allowed hDF attachment and growth, albeit with variable degree of efficiency. Gross visual assessment (Supplementary Fig. S8 and Fig. 1A) did not reveal any morphological differences as a function of substrates' rigidity. Maybe, the most notable observations are that at day 7, longest timepoint assessed, only the PGCL/10/90 and the PLTMC 80/20 had significantly ($p < 0.01$) higher and the PGDTMC 55/15/30 significantly ($p < 0.01$) lower proliferation to TCP and the PGCL 10/90 and PGL 15/85 had significantly ($p < 0.001$) lower and the PGLCLTMC 70/5/15/10 had significantly ($p < 0.001$) higher metabolic activity than TCP.

Direct cultures of the various substrates with THP-1 cells revealed that at day 2, longest timepoint assessed, the PGL 30/70 exhibited significantly ($p < 0.001$) lower cell number compared to normal medium and LPS (Fig. 2A); the PGCL 10/90, PGLCLTMC 70/5/15/10, PGDTMC 55/15/30 and PLTMC 80/20 exhibited significantly ($p < 0.001$) higher metabolic activity compared to normal medium and PGL 30/70 showed significantly ($p < 0.001$) lower metabolic activity compared to LPS (Fig. 2B); the PGLCLTMC 70/5/15/10 and PGDTMC 55/15/30 significantly ($p < 0.001$) higher % of elongated cells than normal medium and all polymers exhibited significantly ($p < 0.001$) lower % of elongated cells than LPS (Fig. 2C and Supplementary Fig. S9).

Indirect cultures of THP-1 cells revealed that at day 2, longest timepoint assessed, the PGL 15/85 and PGL 30/70 groups exhibited

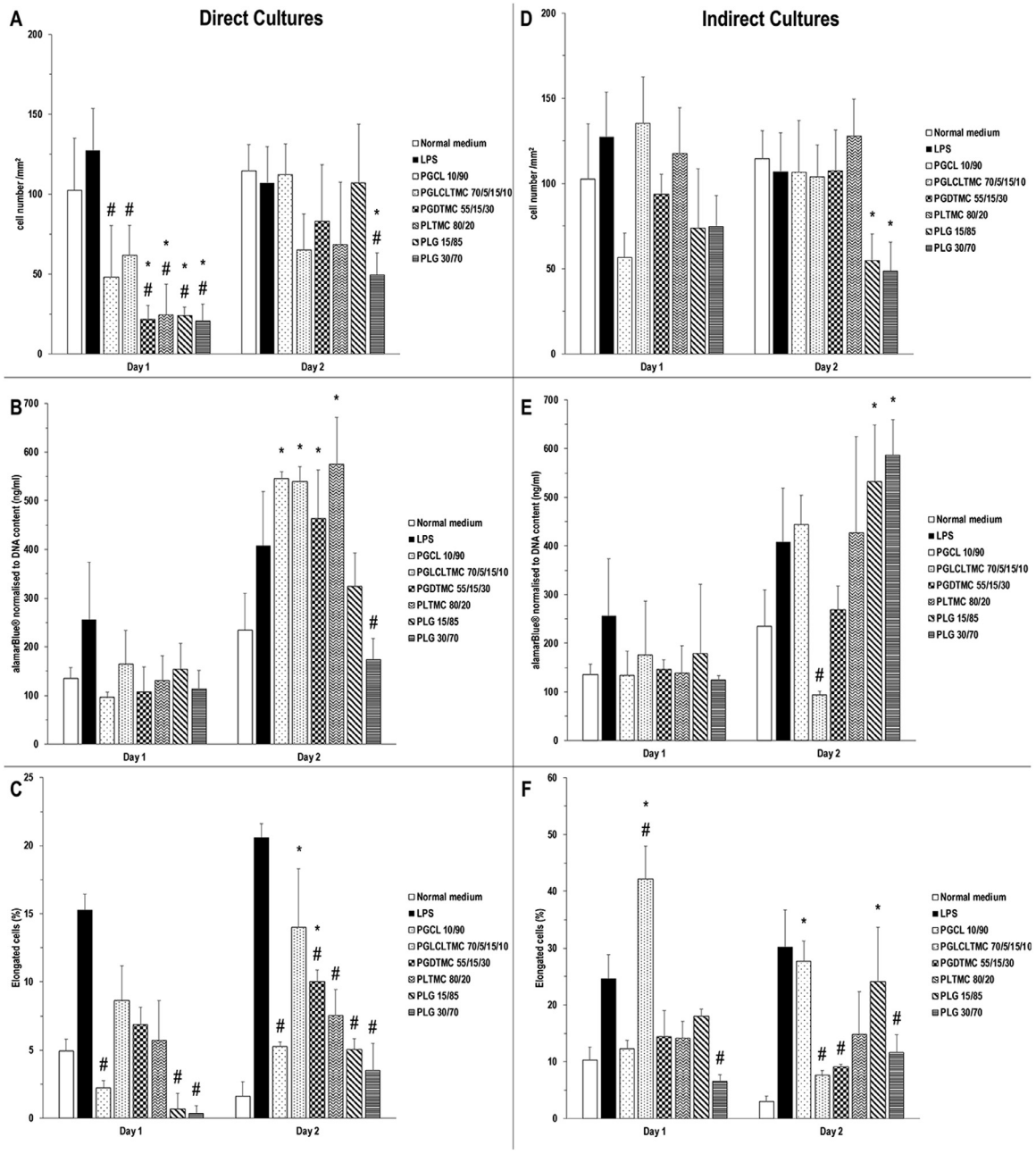

Fig. 2. A polymer-dependent THP-1 proliferation (A: direct culture, D: indirect culture), metabolic activity (B: direct culture, E: indirect culture) and elongation (C: direct culture, F: indirect culture) was observed. * indicates significant difference at $p < 0.001$ between a group and normal medium at a given timepoint. # indicates significant difference at $p < 0.001$ between a group and LPS at a given timepoint.

significantly ($p < 0.01$) lower cell number compared to normal media and LPS (Fig. 2D); the PGL 15/85 and PGL 30/70 exhibited significantly ($p < 0.001$) higher metabolic activity compared to normal medium and the PGLCLTMC 70/5/15/10 exhibited significantly ($p < 0.001$) lower metabolic activity compared to LPS (Fig. 2E); and the PGCL 10/90 and PGL 15/85 exhibited significantly ($p < 0.001$) higher % of elongated cells compared to normal medium and the PGLCLTMC 70/5/15/10, PGDTMC 55/15/30 and PGL 30/70 exhibited significantly ($p < 0.001$) lower % of elongated cells compared to LPS (Fig. 2F and Supplementary Fig. S9).

At day 2, clusters were observed more frequently in LPS and PGL 30/70 in direct culture whilst in indirect culture the presence of clusters was evident in PGL 30/70 and PGLCLTMC 70/5/15/10 groups (Supplementary Fig. S9).

4. Discussion

Over the years, it has been well-established in the literature and clinical practice the importance to as closely as possible match the mechanical properties of implantable devices [13–16] and cell culture substrates [35–38] to the mechanical properties of the tissue and the tissue that the cells were extracted from or intended to be implanted, respectively, for maximisation of their therapeutic potential. In particular, with respect to cell culture substrates, it is worth noting that the vast majority of the work that has been conducted to-date to assess the influence of substrate rigidity on cell response has been based on non-degradable substrates [poly(dimethylsiloxane) or poly(acrylamide) [39,40]] that neither imitate the biomechanical properties of native tissues nor consti-

tute part of any implantable medical device. Herein, we ventured to study six polymer compositions using different combinations of five aliphatic polyester monomers (glycolide, ε-caprolactone, lactide, trimethylene carbonate and dioxanone) that collectively represent the lion's share of raw materials used in the development of synthetic implantable devices.

Starting with the chemical characterisation, similar to previously published NMR spectra for PGCL [41], PGLCLTMC [42], PGDTMC [43], PLTMC [44] and PGL [45] were obtained. The composition of the polymeric films was confirmed by FTIR analysis, indicating that the manufacturing process did not cause any changes to the polymers, as the heating step during compression moulding was short and the temperatures used were closed to the melting temperature of the polymers [46, 47]. These data further advocate the use of compression moulding in medical device fabrication, as a scalable, reproducible and low toxicity (solvent-free) method [48].

GPC analysis revealed that the PLTMC 80/20 had the most monodisperse profile, in comparison to the other polymeric films, as judged by PDI < 2 [49]. Regarding the thermal properties of the studied polymers, PLTMC 80/20 exhibited a difference in its pellet and film DSC curves, where an increase of crystallinity content is due to the compression moulding conditions. Thermal behaviour analysis revealed that pellets and films of PGL 15/85 and PGL 30/70 had glass transition temperatures above 50°C and no melting curve, indicating that these polymers were in amorphous state at room temperature. These data are in agreement with previous studies, where PGL polymers with lactide content higher than 25 % are amorphous in nature [50]. With almost similar lactide content between PGL 15/85 and PLTMC 80/20, the latter showed a decreased T_g and the presence of a melting endotherm event, which can be attributed to the plasticisation effect of poly(trimethylene carbonate) [28]. Polymers with no or low lactide content (e.g. PGCL 10/90, PGLCLTMC 70/5/15/10, PGDTMC 55/15/30) showed T_g below 25°C and melting endothermic event, indicative of a more crystalline structure at room temperature [51]. Furthermore, the high content of poly(ε-caprolactone) (a semi-crystalline polymer) in PGCL 10/90 caused an increased crystallinity content, which is in agreement with previous studies, where copolymers with higher amount of ε-caprolactone had lower T_g and induced higher plasticisation effect [52]. Essentially, the addition of poly(ε-caprolactone) and poly(trimethylene carbonate) to the other aliphatic polyesters makes the polymer structure less ordered and therefore more difficult for the chains to fit closely together. This softens the polymer, lowers the T_g, increases crystallinity content, lowers rigidity and increases elongation at break [53].

The wettability of the produced films was examined using as reference water (polar) and diiodomethane (non-polar). For all polymers, the contact angles were higher in water than in diiodomethane, which is in accordance to the liquid surface tension theory [54] that the largest contact angles are measured for water and the smallest ones correspond to diiodomethane [55]. All polymeric films exhibited contact angle values that are considered hydrophilic [56,57], which contradicts previous observations, where lactide [58], glycolide [59] and trimethylene carbonate [60] polymers were described as hydrophobic. These differences may be attributed to various factors, including the polymerisation, compression and moulding processes; the sample thickness; and the conjugation with known hydrophilic polymers, such as dioxanone [61]. The PGLCLTMC 70/5/15/10 film exhibited the lowest contact angle and the highest surface energy. We believe that this hydrophilicity derives from the reduced surface roughness, which pays an important role in the wettability of a polymer [62,63].

In general, DMA revealed that the storage and loss moduli of the polymeric films were not affected in dry state by frequency at both temperatures tested, indicating that the polymeric films showed resistance to cyclic tension up to 10 Hz. However, the increase in temperature from 25 °C to 37 °C decreased storage and loss moduli of PGLCLTMC 70/5/15/10 and PGDTMC 55/15/30, which can be attributed to the increased flexibility of their polymeric chains with increasing temperatures, as their T_g is below 25 °C. This can be substantiated considering that as the temperature increases, the polymer acquires sufficient internal energy to allow its chains to perform translational and rotational movements, allowing their conformational change [64–66]. Further, when a polymer is above its T_g, the flexibility of its chain depends on the mobility generated by the amorphous phase, whilst when it is below its T_g, the polymer is in the glassy state, and is hard and brittle like a glass [67,68]. The PGLCLTMC 70/5/15/10 also exhibited the highest loss modulus values, indicative of its high viscus profile, due to the combinatory effect of the two plasticising monomers (ε-caprolactone and trimethylene carbonate) that have been shown to increase the viscous response of copolymers [69]. The PGCL 10/90 exhibited the lowest storage and loss moduli for all experimental conditions, which can be explained considering that its T_g and T_m were below 37 °C and therefore the polymer was already at its most relaxed and flexible state. The PGL 15/85 and PGL 30/70 had the highest T_g and storage modulus values at 25 °C and 37 °C, which is in agreement to previous reports, where the amorphous region of lactide and glycolide monomers formed links between stereo-complex crystallites and resulted in increased storage modulus [70]. With respect to PGL 30/70, hydration resulted in decreased storage modulus and increased loss modulus, which can be attributed to brittle behaviour of the glycolide and the softening (becoming more viscus) of the lactide, as has been previously reported [45].

In the study of a biomaterial for tissue engineering applications, it is essential to understand their potential to endure load present in the native tissue, and also to predict the effect that the biomaterial will have to the surrounding matrix. Literature has shown that native tissues show marginally different magnitude of mechanical properties at their macro- and nano-scale [71]. The mechanical properties of the produced films were assessed using macro- (10^{-3} – 10^{-1} m, uniaxial tensile test) and nano- (10^{-6} – 10^{-4} m, nanoindentation) techniques to fully elucidate the potential of the scaffolds as implantable devices and as cell culture substrates, respectively. The classical understanding of elastic behaviour of structures and materials, where the Young's modulus is a material property that does not depend on size and structures follow standard Hooke's law and Euler-Bernoulli theory. Young's Modulus is a fundamental mechanical property that affects the stiffness and for macroscopic structures, it is considered as a bulk material property, independent of size that can be obtain using uniaxial mechanical tests. However, nanoscale physical properties of materials, such as mechanical, electrical and thermal properties, can be different from the bulk values as observed in this work [72]. AFM can provide information about the mechanical properties of a surface at a length scale that is limited only by the dimensions of the AFM tip. When probing mechanical properties, the attractive and repulsive force interactions between the tip and sample are monitored [73]. Measurements at such low levels are of particular importance to assess and understand cell responses to substrate elasticity, as cells sense matrix elasticity at molecular scale level via activation of mechanotransduction signalling pathways [e.g. focal adhesion kinase (FAK) and Rho-associated protein kinase (ROCK)] that control several cellular functions, including morphology, adhesion, proliferation, spreading, migration and differentiation [74–76].

Mechanical properties assessment revealed that PGL 30/70, PGL 15/85 and PLTMC 80/20 films yielded higher Young's modulus, ultimate tensile strength and toughness values and lower strain at break values than PGCL 10/90, PGLCLTMC 70/5/15/10 and PGDTMC

55/15/30 films, which can be attributed to the presence of plasticising monomers (i.e. ε-caprolactone and trimethylene carbonate) in the latter [77] and brittle monomers (i.e. lactide and glycolide) in the former [59,78]. In general, the lactide and glycolide monomers exhibit high rigidity and poor flexibility, which restrict their utilisation in tissue engineering applications that mechanical fatigue resistance is essential [4,79,80]. On the other hand, the poly(ε-caprolactone) is very flexible and degrades slowly (complete degradation beyond 2 years), which restricts its use for tissue engineering applications that a temporary replacement is needed [9,81]. These precise observations triggered investigations into copolymers with trimethylene carbonate [82,83] and dioxanone [61,84,85] to finetune device and tissue mechanical properties / requirements.

The degradation profile of the polymeric films in PBS for up to 21 days was assessed by measuring changes in pH; thermal and mechanical properties; NMR spectra; and M_w and M_n changes with GPC. The by-products of polyester degradation are acidic in nature, resulting in pH drop. The PGCL 10/90 and PLTMC 80/20 films were more resistant to degradation, largely attributed to the ε-caprolactone and trimethylene carbonate content. Previous studies have shown poly(ε-caprolactone) to have slow hydrolytic degradation, which makes it very popular for long-term implants and slow releasing drug delivery applications [86]. Trimethylene carbonate degrades via surface erosion mechanism with non-acidic degradation products and is resistant to nonenzymatic hydrolysis [5,8], which essentially means that its integrity is maintained during degradation [60,87]. The fast degradation of PGLCLTMC 70/5/15/10 and PGDTMC 55/15/30 is attributed to high glycolide content, which is highly susceptible to the action of water [88]. *In vivo,* glycolide degrades in 2 to 4 weeks, losing 60 % of its mass during the first two weeks [89]. NMR analysis detected a significant change in the monomer composition on PGL 30/70 after 21 days degradation. As degradation is associated with changes in the chemical and/or physical structure of a polymer chain and decreased M_w [90], the drastic reduction of the M_w of the PGLCLTMC 70/5/15/10 and PGDTMC 55/15/30 indicates a significant degradation and loss of the polymers' properties. The rapid degradation of glycolide resulted in increase in the crystallinity content of PGLCLTMC 70/5/15/10 and PGL 30/70, whilst PGL 15/85 remained amorphous with no evidence of degradation up to 21 days. The different degradation profiles of PGL 30/70 and PGL 15/85 can be attributed to the different percentage of lactide present. Considering that PLG biodegrades by hydrolysis of its ester linkages [91], the presence of methyl side groups in lactide makes it more hydrophobic than glycolide and hence lactide rich PLG copolymers are less hydrophilic, absorb less water and subsequently degrade more slowly [59].

Biological analysis using hDFs revealed that all substrates supported their growth for up to 7 days in culture (longer timepoint assessed), albeit with variable degree of efficiency. As AFM analysis indicated that all substrates were of similar surface roughness, the observed differences can be attributed to chemical mechanical / composition and/or degradation properties, with most likely the degradation / acidic profile to be the driving force. After 7 days of culture, PGCL 10/90 and PLTMC 80/20, which also exhibited good resistance to degradation, exhibited the highest proliferation, as has been previously reported [44,92,93], whilst the PGDTMC 55/15/30 exhibited an inhibited proliferation effect derived from its early degradation profile. Also, the fast degrading PGLCLTMC 70/5/15/10 exhibited higher metabolic activity than the more stable polymeric films, possibly due to cell stress. Such a behaviour has been previously reported for hDFs, when induced into quiescence via contact inhibition [94]. Whilst the sensitivity of fibroblasts to mechanical cues has been described in the literature [95,96], the rigidity of the polymeric films did not appear to affect hDF morphology, which is a known indicator of cell response to substrate rigidity [97–101] and may be attributed to the high cell density used herein, which has been shown to override the effect of substrate stiffness on cell morphology [102].

Regarding *in vitro* immune response, our data indicate that THP-1 cells cultured on softer polymeric films (e.g. PGCL 10/90) exhibited higher proliferation and metabolic activity in comparison to THP-1 cells cultured to stiffer substrates (e.g. PGL 30/70). Elongated cells quantification supports this trend, with a smaller number of elongated cells on stiff polymers, indicative of a pro-inflammatory potential. Degradation cannot be excluded as a factor of immune response. For example, the highest number of elongated cells was detected for PGLCLTMC 70/5/15/10 at day 2 (during both direct and indirect THP-1 cultures), which can be attributed to its fast degradation profile. At day 2 of the indirect culture, PGCL 10/90 and PGL 15/85 extracts showed a similar higher number of elongated cells compared to normal medium, indicative of an anti-inflammatory behaviour, which could be explained by their slow degradation profiles. These observations are in accordance to previous work that has shown inflammatory response to be affected by chemical signals [103], cross-linking density [34,104] and substrate stiffness [105,106]. In fact, it has been shown that stiff gels (~1.7 MPa) prime macrophages towards a pro-inflammatory phenotype, whilst soft gels (~3.3 kPa) prime cells towards an anti-inflammatory phenotype with an increased capacity of phagocytosis, migration and an amoeboid migration mode [107].

5. Conclusions

Implantable device and tissue / cell mechanical properties mismatch is a common reason for device failure in clinical practice and loss of cell phenotype and function during *in vitro* culture. Further, for *ex vivo* cell expansion, non-degradable polymers with mechanical properties well above most tissues in the body are customarily and erroneously utilised. Herein, we fabricated biodegradable polyester films using compression moulding with a thermal presser. Data obtained clearly illustrate that by appropriately selecting the ratio of the polymeric materials' building blocks (i.e. lactide, glycolide, trimethylene carbonate, dioxanone, ε-caprolactone monomers), substrates with tunable biochemical, biophysical and biological properties can be fabricated to match the properties of a wide range of tissues and cells thereof.

Author contribution

Sofia Ribeiro and Dimitrios I. Zeugolis designed the study and edited and wrote the manuscript. Sofia Ribeiro carried out experiments and analysed data. Ana M. Carvalho performed mechanical analysis using AFM. All authors have approved the manuscript.

Declaration of Competing Interest

Sofia Ribeiro was an early career researcher recruited at Sofradim Production, Medtronic, France and registered for PhD at NUI Galway, Ireland. Yves Bayon is an employee of Sofradim Production, Medtronic, France. Ana M. Carvalho, Emanuel M. Fernandes, Manuela E. Gomes, Rui L. Reis and Dimitrios I. Zeugolis declare no conflicts of interest.

Acknowledgements

This work has received funding from the European Union's Horizon 2020 research and innovation programme under the Marie Skłodowska-Curie, grant agreement no. 676338; the Widespread: Twinning, grant agreement no. 810850; and the European Research Council (ERC) under the European Union's Horizon 2020 research

and innovation programme, grant agreement no. 866126. This work was also supported by Science Foundation Ireland, Career Development Award, grant agreement no. 15/CDA/3629 and Science Foundation Ireland / European Regional Development Fund, grant agreement no. 13/RC/2073. We would also like to thank Darlene Nebinger, Danielle Lord and Oswaldo Fabian from Medtronic North Haven, USA, for all their technical / experimental support.

Supplementary materials

Supplementary material associated with this article can be found, in the online version, at doi:10.1016/j.actbio.2020.11.026.

References

[1] T.K. Dash, V.B. Konkimalla, Poly-ϵ-caprolactone based formulations for drug delivery and tissue engineering: a review, J. Control Release 158 (2012) 15–33.
[2] F.A.M.M. Gonçalves, A.C. Fonseca, M. Domingos, A. Gloria, A.C. Serra, J.F.J. Coelho, The potential of unsaturated polyesters in biomedicine and tissue engineering: synthesis, structure-properties relationships and additive manufacturing, Prog. Polym. Sci. 68 (2017) 1–34.
[3] S. Tajbakhsh, F. Hajiali, A comprehensive study on the fabrication and properties of biocomposites of poly(lactic acid)/ceramics for bone tissue engineering, Mater. Sci. Eng. C Mater. Biol. Appl. 70 (2017) 897–912.
[4] N. Goonoo, R. Jeetah, A. Bhaw-Luximon, D. Jhurry, Polydioxanone-based bio–materials for tissue engineering and drug/gene delivery applications, Eur. J. Pharm. Biopharm. 97 (2015) 371–391.
[5] K. Fukushima, Poly(trimethylene carbonate)-based polymers engineered for biodegradable functional biomaterials, Biomater. Sci. 4 (2016) 9–24.
[6] H. Tian, Z. Tang, X. Zhuang, X. Chen, X. Jing, Biodegradable synthetic polymers: preparation, functionalization and biomedical application, Prog. Polym. Sci. 37 (2012) 237–280.
[7] A.L. Sisson, M. Schroeter, A. Lendlein, Handbook of Biodegradable Polymers, Wiley-VCH Verlag GmbH & Co, 2011.
[8] H. Ye, K. Zhang, D. Kai, Z. Li, X.J. Loh, Polyester elastomers for soft tissue engineering, Chem. Soc. Rev. 47 (2018) 4545–4580.
[9] Q. Chen, S. Liang, G.A. Thouas, Elastomeric biomaterials for tissue engineering, Prog. Polym. Sci. 38 (2013) 584–671.
[10] K.E. Washington, R.N. Kularatne, V. Karmegam, M.C. Biewer, M.C. Stefan, Recent advances in aliphatic polyesters for drug delivery applications, WIRE Nanomed. Nanobiotechnol. 9 (2016) e1146–e1161.
[11] H.R. Ihre, O.L.P. De Jesús, F.C. Szoka, J.M.J. Fréchet, Polyester dendritic systems for drug delivery applications: design, synthesis, and characterization, Bioconjugate Chem. 13 (2002) 443–452.
[12] I. Manavitehrani, A. Fathi, H. Badr, S. Daly, A. Negahi Shirazi, F. Dehghani, Biomedical applications of biodegradable polyesters, Polymers (Basel) 8 (2016) 20–52.
[13] M. Vatankhah-Varnosfaderani, W.F.M. Daniel, M.H. Everhart, A.A. Pandya, H. Liang, K. Matyjaszewski, A.V. Dobrynin, S.S. Sheiko, Mimicking biological stress-strain behaviour with synthetic elastomers, Nature 549 (2017) 497–501.
[14] S. Prasadh, R.C.W. Wong, Unraveling the mechanical strength of biomaterials used as a bone scaffold in oral and maxillofacial defects, Oral Sci. Int. 15 (2018) 48–55.
[15] M. Gasik, A. Zuhlke, A.M. Haaparanta, V. Muhonen, K. Laine, Y. Bilotsky, M. Kellomaki, I. Kiviranta, The importance of controlled mismatch of biomechanical compliances of implantable scaffolds and native tissue for articular cartilage regeneration, Front. Bioeng. Biotechnol. 6 (2018) 187.
[16] H. Petit-Eisenmann, E. Epailly, M. Velten, J. Radojevic, B. Eisenmann, H. Kremer, M. Kindo, Impact of prosthesis-patient mismatch on long-term functional capacity after mechanical aortic valve replacement, Can. J. Cardiol. 32 (2016) 1493–1499.
[17] H. Lv, H. Wang, Z. Zhang, W. Yang, W. Liu, Y. Li, L. Li, Biomaterial stiffness determines stem cell fate, Life Sci. 178 (2017) 42–48.
[18] A.J. Engler, S. Sen, H.L. Sweeney, D.E. Discher, Matrix elasticity directs stem cell lineage specification, Cell 126 (2006) 677–689.
[19] N. Bouchonville, M. Meyer, C. Gaude, E. Gay, D. Ratel, A. Nicolas, AFM mapping of the elastic properties of brain tissue reveals kPa/μm gradients of rigidity, Soft Matter 12 (2016) 6232–6239.
[20] C. Then, J. Menger, G. Benderoth, M. Alizadeh, T.J. Vogl, G. Silber, A method for a mechanical characterisation of human gluteal tissue, Technol. Health Care 15 (2007) 385–398.
[21] L. Penuela, C. Negro, M. Massa, E. Repaci, E. Cozzani, A. Parodi, S. Scaglione, R. Quarto, R. Raiteri, Atomic force microscopy for biomechanical and structural analysis of human dermis: A complementary tool for medical diagnosis and therapy monitoring, Exp. Dermatol. 27 (2018) 150–155.
[22] P.F. Lozano, M. Scholze, C. Babian, H. Scheidt, F. Vielmuth, J. Waschke, B. Ondruschka, N. Hammer, Water-content related alterations in macro and micro scale tendon biomechanics, Sci. Rep. 9 (2019) 7887.
[23] M. Kwacz, Z. Rymuza, M. Michalowski, J. Wysocki, Elastic properties of the annular ligament of the human stapes-AFM measurement, J. Assoc. Res. Otolaryngol. 16 (2015) 433–446.
[24] M. Stolz, R. Raiteri, A.U. Daniels, M. VanLandingham, W.Baschong R., U. Aebi, Dynamic elastic modulus of porcine articular cartilage determined at two different levels of tissue organization by indentation-type atomic force microscopy, Biophys. J. 86 (2004) 3269–3283.
[25] S. Hengsberger, A. Kulik, P. Zysset, A combined atomic force microscopy and nanoindentation technique to investigate the elastic properties of bone structural units, Eur. Cell Mater. 1 (2001) 12–17.
[26] P.M. Gilbert, K.L. Havenstrite, K.E.G. Magnusson, A. Sacco, N.A. Leonardi, P. Kraft, N.K. Nguyen, S. Thrun, M.P. Lutolf, H.M. Blau, Substrate elasticity regulates skeletal muscle stem cell self-renewal in culture, Science 329 (2010) 1078–1081.
[27] J.J. Wurth, N.R. Blumenthal, V.P. Shastri, Hydrophilization of poly(caprolactone) copolymers through introduction of oligo(ethylene glycol) moieties, PLoS One 9 (2014) e99157.
[28] Y. Qin, J. Yang, M. Yuan, J. Xue, J. Chao, Y. Wu, M. Yuan, barrier Mechanical, and thermal properties of poly(lactic acid)/poly(trimethylene carbonate)/talc composite films, J. Appl. Polym. Sci. 131 (2014) 40016–44022.
[29] A. Kiersnowski, M. Kozak, S. Jurga, J. Pigłowski, Structure and crystallization behaviour of poly(ε-caprolactone)/clay intercalated nanocomposites, Polym. Polym. Comp. 12 (2004) 727–737.
[30] C. Nakafuku, H. Yoshimura, Melting parameters of poly(glycolic acid), Polymer 45 (2004) 3583–3585.
[31] D.K. Owens, R.C. Wendt, Estimation of the surface free energy of polymers, J. Appl. Polym. Sci. 13 (1969) 1741–1747.
[32] A. Azeem, L. Marani, K. Fuller, K. Spanoudes, A. Pandit, D.I. Zeugolis, Influence of nonsulfated polysaccharides on the properties of electrospun poly(lactic-co-glycolic acid) fibers, ACS Biomater. Sci. Eng. 3 (2017) 1304–1312.
[33] H. Capella-Monsonis, J. Kelly, S. Kearns, D.I. Zeugolis, Decellularised porcine peritoneum as a tendon protector sheet, Biomed. Mater. 14 (2019) 044102.
[34] L.M. Delgado, K. Fuller, D.I. Zeugolis, Collagen cross-linking: Biophysical, biochemical, and biological response analysis, Tissue Eng. A 23 (2017) 1064–1077.
[35] M.H. Lee, P.H. Wu, J.R. Staunton, R. Ros, G.D. Longmore, D. Wirtz, Mismatch in mechanical and adhesive properties induces pulsating cancer cell migration in epithelial monolayer, Biophys. J. 102 (2012) 2731–2741.
[36] I.L. Ivanovska, J. Swift, K. Spinler, D. Dingal, S. Cho, D.E. Discher, Cross-linked matrix rigidity and soluble retinoids synergize in nuclear lamina regulation of stem cell differentiation, Mol. Biol. Cell 28 (2017) 2010–2022.
[37] A.R. Killaars, J.C. Grim, C.J. Walker, E.A. Hushka, T.E. Brown, K.S. Anseth, Extended exposure to stiff microenvironments leads to persistent chromatin remodeling in human mesenchymal stem cells, Adv. Sci. (Weinh) 6 (2018) 1801483–1801495.
[38] J.M. Collins, P. Ayala, T.A. Desai, B. Russell, Three-dimensional culture with stiff microstructures increases proliferation and slows osteogenic differentiation of human mesenchymal stem cells, Small 6 (2010) 355–360.
[39] Z. Li, Y. Gong, S. Sun, Y. Du, D. Lu, X. Liu, M. Long, Differential regulation of stiffness, topography, and dimension of substrates in rat mesenchymal stem cells, Biomaterials 34 (2013) 7616–7625.
[40] D. Lu, C. Luo, C. Zhang, Z. Li, M. Long, Differential regulation of morphology and stemness of mouse embryonic stem cells by substrate stiffness and topography, Biomaterials 35 (2014) 3945–3955.
[41] S.H. Lee, B.S. Kim, S.H. Kim, S.W. Choi, S.I. Jeong, I.K. Kwon, S.W. Kang, J. Nikolovski, D.J. Mooney, Y.K. Han, Y.H. Kim, Elastic biodegradable poly(glycolide-co-caprolactone) scaffold for tissue engineering, J. Biomed. Mater. Res. A 66 (2003) 29–37.
[42] R.F. Storey, T.P. Hickey, Degradable polyurethane networks based on D,L-lactide, glycolide, e-caprolactone, and trymethylene carbonate homopolyester and copolyester triols, Polymer 35 (1994) 830.
[43] J. Yang, F. Liu, L. Yang, S. Li, Hydrolytic and enzymatic degradation of poly(trimethylene carbonate-co-d,l-lactide) random copolymers with shape memory behavior, Eur. Polym. J. 46 (2010) 783–791.
[44] L.J. Ji, K.L. Lai, B. He, G. Wang, L.Q. Song, Y. Wu, Z.W. Gu, Study on poly(L-lactide-co-trimethylene carbonate): synthesis and cell compatibility of electrospun film, Biomed. Mater. 5 (2010) 045009.
[45] C. D'Avila Carvalho Erbetta, R.J. Alves, J.M. Resende, R.F.d.S. Feritas, R.G. de Sousa, Synthesis and characterization of poly(D,L-lactide-co-glycolide) copolymer, J. Biomater. Nanobiotechnol. 03 (2012) 208–225.
[46] I. Zembko, I. Ahmed, A. Farooq, J. Dail, P. Tawari, W. Wang, C. McConville, Development of disulfiram-loaded poly(lactic-co-glycolic acid) wafers for the localised treatment of glioblastoma multiforme: a comparison of manufacturing techniques, J. Pharm. Sci. 104 (2015) 1076–1086.
[47] H. Little, S.A. Clarke, E. Cunningham, F. Buchanan, Process-induced degradation of bioresorbable PDLGA in bone tissue scaffold production, J. Mater. Sci. Mater. Med. 29 (2017) 14–23.
[48] A.J. Hulme, T.C. Goodhead, Cost effective reprocessing of polyurethane by hot compression moulding, J. Mater. Process. Technol. 139 (2003) 322–326.
[49] I.M. Mahbubul, in: 1 - Introduction to Nanofluid, Preparation, Characterization, Properties and Application of Nanofluid, William Andrew Applied Sciences Piblishers, 2019, pp. 1–13.
[50] M. Ayyoob, Y.J. Kim, Effect of chemical composition variant and oxygen plasma treatments on the wettability of PLGA thin films, synthesized by direct copolycondensation, Polymers (Basel) 10 (2018) 1132–1147.
[51] J.M. Hutchinson, Interpretation of structural recovery of amorphous polymers from DSC data, in: J.F. Janssson, U.W. Gedde (Eds.), Solidification Processes in Polymers, Steinkopff, Darmstadt, 1992, pp. 68–73.

[52] M. Rizzuto, A. Mugica, M. Zubitur, D. Caretti, A.J. Müller, Plasticization and anti-plasticization effects caused by poly(lactide-ran-caprolactone) addition to double crystalline poly(l-lactide)/poly(ε-caprolactone) blends, Cryst. Eng. Comm. 18 (2016) 2014–2023.
[53] E.H. Immergut, H.F. Mark, Principles of Plasticization, in: N.A.J. Platzer (Ed.), Plasticization and Plasticizer Processes, American Chemical Society, 1965, pp. 1–26.
[54] J.G. Kirkwood, F.P. Buff, The statistical mechanical theory of surface tension, J. Chem. Phys. 17 (1949) 338–340.
[55] A. Cammarano, G. De Luca, E. Amendola, Surface modification and adhesion improvement of polyester films, Cent. Eur. J. Chem. 11 (2013) 35–45.
[56] K.Y. Law, Definitions for hydrophilicity, hydrophobicity, and superhydrophobicity: getting the basics right, J. Phys. Chem. Lett. 5 (2014) 686–688.
[57] E.I. Vargha-Butler, E. Kiss, C.N.C. Lam, Z. Keresztes, E. Kálmán, L. Zhang, A.W. Neumann, Wettability of biodegradable surfaces, Colloid Polym. Sci. 279 (2001) 1160–1168.
[58] A. Bakry, M.S.A. Darwish, A.M.A. El Naggar, Assembling of hydrophilic and cytocompatible three-dimensional scaffolds based on aminolyzed poly(l-lactide) single crystals, New J. Chem. 42 (2018) 16930–16939.
[59] H.K. Makadia, S.J. Siegel, Poly lactic-co-glycolic acid (PLGA) as biodegradable controlled drug delivery carrier, Polymers (Basel) 3 (2011) 1377–1397.
[60] Z. Zhang, R. Kuijer, S.K. Bulstra, D.W. Grijpma, J. Feijen, The in vivo and in vitro degradation behavior of poly(trimethylene carbonate), Biomaterials 27 (2006) 1741–1748.
[61] A. Ahlinder, T. Fuoco, A. Finne-wistrand, Medical grade polylactide, copolyesters and polydioxanone: Rheological properties and melt stability, Polym. Test. 72 (2018) 214–222.
[62] H. Fan, Z. Guo, Bioinspired surfaces with wettability: Biomolecules adhesion behaviors, Biomater. Sci. 8 (2020) 1502–1535.
[63] K.J. Kubiak, M.C.T. Wilson, T.G. Mathia, P. Carval, Wettability versus roughness of engineering surfaces, Wear 271 (2011) 523–528.
[64] P.H. Daniels, A. Cabrera, Plasticizer compatibility testing: Dynamic mechanical analysis and glass transition temperatures, J. Vinyl Addit. Techn. 21 (2015) 7–11.
[65] E.M. Mahdi, J.-C. Tan, Dynamic molecular interactions between polyurethane and ZIF-8 in a polymer-MOF nanocomposite: microstructural, thermo-mechanical and viscoelastic effects, Polymer 97 (2016) 31–43.
[66] A.C. de Paula, F. Uliana, E.A. da Silva Filho, K. Soares, P.P. Luz, Use of DMA-material pocket to determine the glass transition temperature of nitrocellulose blends in film form, Carbohydr. Polym. 226 (2019) 115288–115292.
[67] N. Saba, M. Jawaid, A review on thermomechanical properties of polymers and fibers reinforced polymer composites, J. Ind. Eng. Chem. 67 (2018) 1–11.
[68] Y. Zhang, R.D. Adams, L.F.M. da Silva, A rapid method of measuring the glass transition temperature using a novel dynamic mechanical analysis method, J. Adhes. 89 (2013) 785–806.
[69] A. Bergfelt, M.J. Lacey, J. Hedman, C. Sångeland, D. Brandell, T. Bowden, ε-caprolactone-based solid polymer electrolytes for lithium-ion batteries: synthesis, electrochemical characterization and mechanical stabilization by block copolymerization, RSC Adv. 8 (2018) 16716–16725.
[70] Y. Srisuwan, Y. Baimark, Mechanical properties and heat resistance of stereocomplex polylactide/copolyester blend films prepared by in situ melt blending followed with compression molding, HeliyoMn 4 (2018) e01082–e01100.
[71] M. Griffin, Y. Premakumar, A. Seifalian, P.E. Butler, M. Szarko, Biomechanical characterization of human soft tissues using indentation and tensile testing, J. Vis. Exp. 118 (2016) e54872.
[72] L. Qiu, N. Zhu, Y. Feng, E.E. Michaelides, G. Żyła, D. Jing, X. Zhang, P.M. Norris, C.N. Markides, O. Mahian, A review of recent advances in thermophysical properties at the nanoscale: from solid state to colloids, Phys. Rep. 843 (2020) 1–81.
[73] D.C. Hurley, M. Kopycinska-Müller, A.B. Kos, Mapping mechanical properties on the nanoscale using atomic-force acoustic microscopy, JOM 59 (2007) 23–29.
[74] G. De Santis, A.B. Lennon, F. Boschetti, B. Verhegghe, P. Verdonck, P.J. Prendergast, How can cells sense the elasticity of a substrate? An analysis using a cell tensegrity model, Eur. Cell Mater. 22 (2011) 202–213.
[75] A. Higuchi, Q.D. Ling, Y. Chang, S.T. Hsu, A. Umezawa, Physical cues of biomaterials guide stem cell differentiation fate, Chem. Rev. 113 (2013) 3297–3328.
[76] Y.S. Pek, A.C. Wan, J.Y. Ying, The effect of matrix stiffness on mesenchymal stem cell differentiation in a 3D thixotropic gel, Biomaterials 31 (2010) 385–391.
[77] M. Shahrousvand, G.M.M. Sadeghi, E. Shahrousvand, M. Ghollasi, A. Salimi, Superficial physicochemical properties of polyurethane biomaterials as osteogenic regulators in human mesenchymal stem cells fates, Colloids Surf. B 156 (2017) 292–304.
[78] N. Diban, S. Haimi, L. Bolhuis-versteeg, S. Teixeira, S. Miettinen, A. Poot, D. Grijpma, D. Stamatialis, Hollow fibers of poly(lactide-co-glycolide) and poly(e-caprolactone) blends for vascular tissue engineering applications, Acta Biomater. 9 (2013) 6450–6458.
[79] A. Sodergard, M. Stolt, Properties of lactic acid based polymers and their correlation with composition, Prog. Polym. Sci. 27 (2002) 1123–1163.
[80] A.P. Pego, D.W. Grijpma, J. Feijen, Enhanced mechanical properties of 1,3-trimethylene carbonate polymers and networks, Polymer 44 (2003) 6495–6504.
[81] A.R. Webb, J. Yang, G.A. Ameer, Biodegradable polyester elastomers in tissue engineering, Expert Opion Biol. Ther. 4 (2004) 801–812.
[82] Y. Ikada, H. Tsuji, Biodegradable polyesters for medical and ecological applications, Macromol. Rapid Commun. 132 (2000) 117–132.
[83] E. Bat, B.H.M. Kothman, G.A. Higuera, C.A.V. Blitterswijk, J. Feijen, D.W. Grijpma, Biomaterials ultraviolet light crosslinking of poly (trimethylene carbonate) for elastomeric tissue engineering scaffolds, Biomaterials 31 (2010) 8696–8705.
[84] A. Fontana, A. Bistolfi, M. Crova, G. Massazza, Primary stability of a PGLA/Polydioxanone membrane for potential autologous chondrocyte implantation in the hip joint. A cadaveric study, Hip. Int. 23 (2013) 337–342.
[85] T. Fuoco, A. Ahlinder, S. Jain, K. Mustafa, A. Finne-Wistrand, Poly(epsilon-caprolactone-co-p-dioxanone): a degradable and printable copolymer for pliable 3D scaffolds fabrication toward adipose tissue regeneration, Biomacromolecules 21 (2019) 188–198.
[86] C.K. Arakawa, C.A. DeForest, Polymer Design and Development, in: A. Vishwakarma, J.M. Karp (Eds.), Biology and Engineering of Stem Cell Niches, Academic Press, Boston, 2017, pp. 295–314.
[87] E. Bat, Z. Zhang, J. Feijen, D.W. Grijpma, Biodegradable elastomers for biomedical applications and regenerative medicine, Regen. Med. 9 (2014) 385–398.
[88] E.M. Prieto, S.A. Guelcher, Tailoring properties of polymeric biomedical foams, in: P.A. Netti (Ed.), Biomedical Foams for Tissue Engineering Applications, Woodhead Publishing, 2014, pp. 129–162.
[89] D. Gorth, T.J Webster, Matrices for tissue engineering and regenerative medicine, in: M. Lysaght, T.J. Webster (Eds.), Biomaterials for Artificial Organs, Woodhead Publishing, 2011, pp. 270–286.
[90] C.F. Jasso-Gastinel, J.F.A. Soltero-Martínez, E. Mendizábal, in: 1 - Introduction: Modifiable Characteristics and Applications, Modification of Polymer Properties, Elsevier Inc., 2017, pp. 1–21.
[91] P. Gentile, V. Chiono, I. Carmagnola, P.V. Hatton, An overview of poly(lactic-co-glycolic) acid (PLGA)-based biomaterials for bone tissue engineering, Int. J. Mol. Sci. 15 (2014) 3640–3659.
[92] I.K. Kwon, K.D. Park, S.W. Choi, S.H. Lee, E.B. Lee, J.S. Na, S.H. Kim, Y.H. Kim, Fibroblast culture on surface-modified poly(glycolide-co-epsilon-caprolactone) scaffold for soft tissue regeneration, J. Biomater. Sci. Polym. Ed. 12 (2001) 1147–1160.
[93] B.L. Dargaville, C. Vaquette, H. Peng, F. Rasoul, Y.Q. Chau, J.J. Cooper-white, J.H. Campbell, A.K. Whittaker, Cross-linked poly(trimethylene carbonate–co-L-lactide) as a biodegradable, elastomeric scaffold for vascular engineering applications, Biomacromolecules 12 (2011) 3856–3869.
[94] J.M. Lemons, X.J. Feng, B.D. Bennett, A. Legesse-Miller, E.L. Johnson, I. Raitman, E.A. Pollina, H.A. Rabitz, J.D. Rabinowitz, H.A. Coller, Quiescent fibroblasts exhibit high metabolic activity, PLoS Biol. 8 (2010) e1000514–e1000529.
[95] D.J. Tschumperlin, Fibroblasts and the ground they walk on, Physiology (Bethesda) 28 (2013) 380–390.
[96] S. Asano, S. Ito, K. Takahashi, K. Furuya, M. Kondo, M. Sokabe, Y. Hasegawa, Matrix stiffness regulates migration of human lung fibroblasts, Physiol. Rep. 5 (2017) e13281.
[97] Y. Ni, M.Y.M. Chiang, Cell morphology and migration linked to substrate rigidity, Soft Matter 3 (2007) 1285–1292.
[98] S. Tee, J. Fu, C. Chen, P. Janmey, Cell shape and substrate rigidity both regulate cell stiffness, Biophys. J. 100 (2011) L25–L27.
[99] A. Jannatbabaei, M. Tafazzoli-Shadpour, E. Seyedjafari, N. Fatouraee, Cytoskeletal remodeling induced by substrate rigidity regulates rheological behaviors in endothelial cells, J. Biomed. Mater. Res. A 107 (2019) 71–80.
[100] T. Yeung, P. Georges, L. Flanagan, B. Marg, M. Ortiz, M. Funaki, N. Zahir, W. Ming, V. Weaver, P. Janmey, Effects of substrate stiffness on cell morphology, cytoskeletal structure, and adhesion, Cell Motil. Cytoskeleton 60 (2005) 24–34.
[101] M. Gupta, B. Doss, L. Kocgozlu, M. Pan, R. Mège, A. Callan-Jones, R. Voituriez, B. Ladoux, Cell shape and substrate stiffness drive actin-based cell polarity, Phys. Rev. E 99 (2019) 012412–012427.
[102] B. Venugopal, P. Mogha, J. Dhawan, A. Majumder, Cell density overrides the effect of substrate stiffness on human mesenchymal stem cells' morphology and proliferation, Biomater. Sci. 6 (2018) 1109–1119.
[103] A. Mantovani, A. Sica, S. Sozzani, P. Allavena, A. Vecchi, M. Locati, The chemokine system in diverse forms of macrophage activation and polarization, Trends Immunol. 25 (2004) 677–686.
[104] S.F. Badylak, J.E. Valentin, A.K. Ravindra, G.P. McCabe, A.M. Stewart-Akers, Macrophage phenotype as a determinant of biologic scaffold remodeling, Tissue Eng. A 14 (2008) 1835–1842.
[105] T. Okamoto, Y. Takagi, E. Kawamoto, E.J. Park, H. Usuda, K. Wada, M. Shimaoka, Reduced substrate stiffness promotes M2-like macrophage activation and enhances peroxisome proliferator-activated receptor gamma expression, Exp. Cell Res. 367 (2018) 264–273.
[106] A.K. Blakney, M.D. Swartzlander, S.J. Bryant, The effects of substrate stiffness on the in vitro activation of macrophages and in vivo host response to poly(ethylene glycol)-based hydrogels, J. Biomed. Mater. Res. A 100 (2012) 1375–1386.
[107] R. Sridharan, B. Cavanagh, A.R. Cameron, D.J. Kelly, F.J. O'Brien, Material stiffness influences the polarization state, function and migration mode of macrophages, Acta Biomater. 89 (2019) 47–59.